An Aromatic Microdomain at the Cannabinoid CB_1 Receptor Constitutes an Agonist/Inverse Agonist Binding Region

Sean D. McAllister,[†] Gulrukh Rizvi,[†] Sharon Anavi-Goffer,[†] Dow P. Hurst,[‡] Judy Barnett-Norris,[‡] Diane L. Lynch,[‡] Patricia H. Reggio,[‡] and Mary E. Abood*[,†]

Forbes Norris ALS/MDA Research Center, California Pacific Medical Center, San Francisco, California 94115, and Department of Chemistry and Biochemistry, Kennesaw State University, 1000 Chastain Rd, Kennesaw, Georgia 30144

Received May 30, 2003

The cannabinoid CB_1 receptor transmembrane helix (TMH) 3−4−5−6 region includes an aromatic microdomain comprised of residues F3.25, F3.36, W4.64, Y5.39, W5.43, and W6.48. In previous work, we have demonstrated that aromaticity at position 5.39 in CB_1 is crucial for proper function of CB_1. Modeling studies reported here suggest that in the inactive state of CB_1, the binding site of the CB_1 inverse agonist/antagonist SR141716A is within the TMH3−4−5−6 aromatic microdomain and involves direct aromatic stacking interactions with F3.36, Y5.39, and W5.43, as well as hydrogen bonding with K3.28. Further, modeling studies suggest that in the active state of CB_1, the CB agonist WIN55,212−2 binds in this same aromatic microdomain, with direct aromatic stacking interactions with F3.36, W5.43, and W6.48. In contrast, in the binding pocket model, the CB agonist anandamide binds in the TMH2−3−6−7 region in which hydrogen bonding and C−H$\cdots\pi$ interactions appear to be important. Only one TMH3 aromatic residue, F3.25, was found to be part of the anandamide binding pocket. To probe the importance of the TMH3−4−5−6 aromatic microdomain to ligand binding, stable transfected cell lines were created for single-point mutations of each aromatic microdomain residue to alanine. Improper cellular expression of the W4.64A was observed and precluded further characterization of this mutation. The affinity of the cannabinoid agonist CP55,940 was unaffected by the F3.25A, F3.36A, W5.43A, or W6.48A mutations, making CP55,940 an appropriate choice as the radioligand for binding studies. The binding of SR141716A and WIN55,212−2 were found to be affected by the F3.36A, W5.43A, and W6.48A mutations, suggesting that these residues are part of the binding site for these two ligands. Only the F3.25A mutation was found to affect the binding of anandamide, suggesting a divergence in binding site regions for anandamide from WIN55,212−2, as well as SR141716A. Taken together, these results support modeling studies that identify the TMH3−4−5−6 aromatic microdomain as the binding region of SR141716A and WIN55,212−2, but not of anandamide.

Introduction

The cannabinoid receptor (CB_1), a member of the G-protein coupled receptor (GPCR) family, can interact with five structurally distinct classes of compounds. These include CB_1 classical cannabinoid agonists [such as (−)-*trans*-Δ-9-tetrahydrocannabinol, Δ^9-THC], nonclassical cannabinoid agonists [such as (1*R*,3*R*,4*R*)-3-[2-hydroxy-4-(1,1-dimethylheptyl)phenyl]-4-(3-hydroxypropyl)cyclohexan-1-ol, CP55,940], endogenous cannabinoid agonists (such as *N*-arachidonoylethanolamine, anandamide), aminoalkylindole (AAI) agonists [such as [2,3-dihydro-5-methyl-3-[(4-morpholinyl)methyl]pyrrolo-[1,2,3-*de*]-1,4-benzoxazin -6-yl](1-naphthyl)methanone, WIN55,212−2], and diaryl pyrazole antagonist/inverse agonists [such as *N*-(piperidin-1-yl)-5-(4-chlorophenyl)-1-(2,4-dichlorophenyl)-4-methyl-1*H*-pyrazole-3-carboxamide, SR141716A] (see Chart 1). There is a rapidly growing understanding of the cannabinoid system as an important endogenous regulator of neuronal, cardiac, reproductive, and immune function.[1] Therefore, there is considerable value in understanding the specific ligand−receptor interactions; this is particularly relevant as compounds are developed for medical intervention.

The CB_2 receptor, whose overall sequence similarity in the transmembrane helices (TMH) is only 68% of CB_1, has been used in chimera studies with CB_1 to probe for receptor-specific ligand interactions.[2,3] These studies suggested that the TMH4-E2-TMH5 region of CB_1 contains residues critical for the binding of the CB_1/CB_2 aminoalkylindole agonist WIN55,212−2 and the CB_1-selective diaryl pyrazole antagonist/inverse agonist SR141716A. Mutation studies have also shown that CB_1/CB_2 subtype differences in TMH3[4] and TMH5[5] contribute to the CB_2 selectivity of WIN55,212−2. A recent mutant cycle study identified K3.28 as an important interaction site for SR141716A at CB_1,[6] while CB_1 Y5.39F/Y5.39I mutation studies have underscored the structural importance of aromaticity at position 5.39.[7] Surprisingly, however, further elaboration of the CB_1 binding site of either SR141716A or WIN55,212−2 through mutation studies has not been reported in the literature.

In the β_2-adrenergic receptor and related aminergic receptors, a highly conserved cluster of aromatic amino acids is found on TMH6 that faces the binding site

* Corresponding author. Phone: (415)-923-3607. Fax: (415)-563-7325. E-mail: mabood@cooper.cpmc.org.
[†] Forbes Norris ALS/MDA Research Center.
[‡] Kennesaw State University.

10.1021/jm0302647 CCC: $25.00
Published on Web 10/23/2003

Chart 1

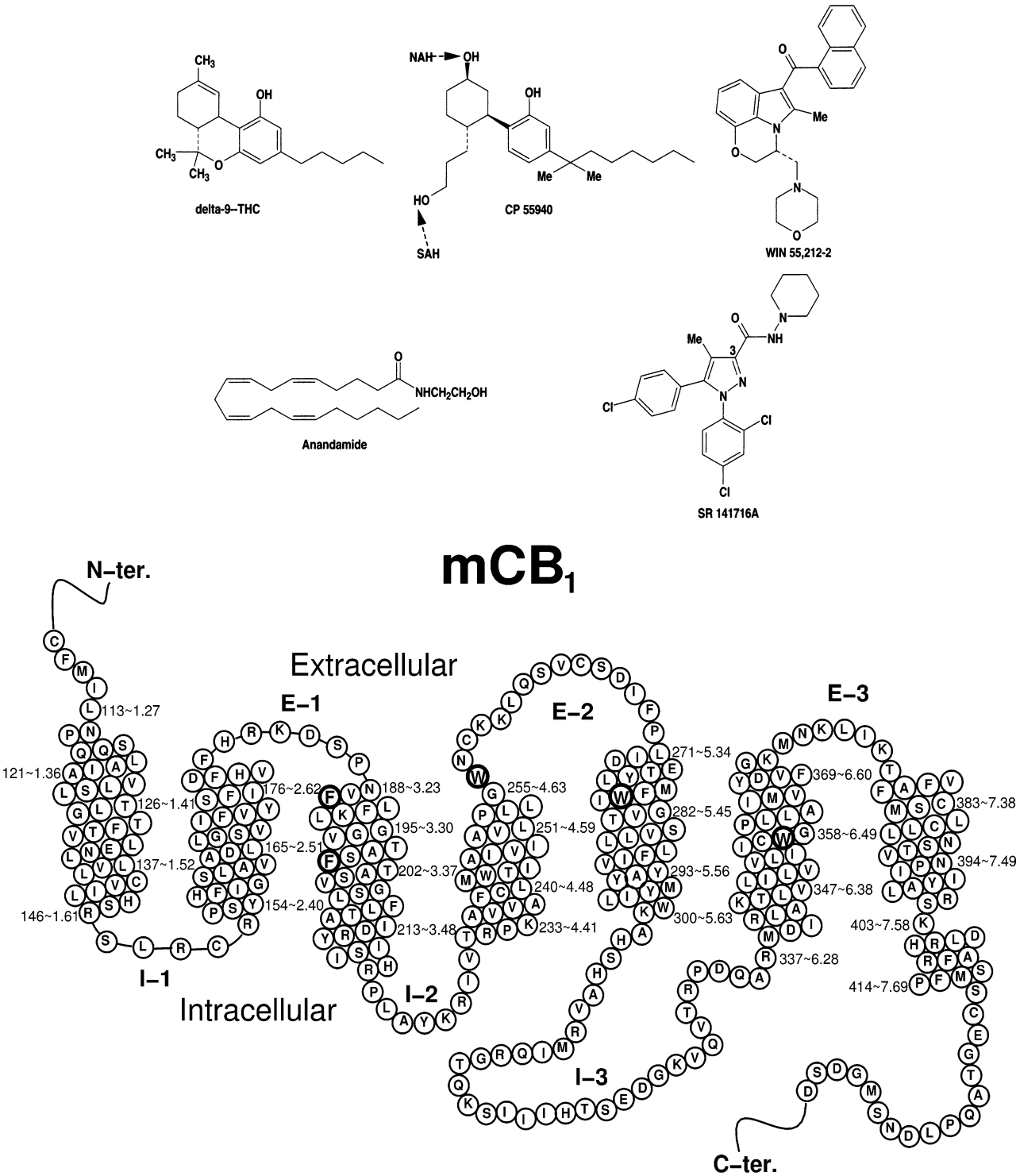

Figure 1. A helix net representation of the sequence of the mouse CB_1 receptor. The amino acids mutated in this study are highlighted in bold.

crevice (F6.44, W6.48, F6.51, and F6.52).[8] The CB_1 receptor lacks this cluster on TMH6 (L6.44, W6.48, L6.51, and L6.52) but contains instead a microdomain of aromatic residues that face into the ligand binding pocket in the TMH3−4−5−6 region, including F3.25, F3.36, W4.64, Y5.39, W5.43, and W6.48 (Figure 1). The importance of Y5.39 for receptor ligand recognition and function in both CB_1 and CB_2 has been recently reported by our group.[7] In this investigation, a Monte Carlo/stochastic dynamics study of CB_1 in its inactive state identified two aromatic subclusters in the TMH3−4−5−6 region of CB_1. The first cluster was a triad (F3.36/W5.43/W6.48) involved in aromatic stacking interactions that appeared to be open for additional interaction with ligand, while the second was Y5.39 and W4.64. This latter cluster appeared to be more important for stabilizing the positions of TMHs 4 and 5 in the TMH bundle on the extracellular side.

We hypothesized that since SR141716A and WIN55,-212−2 are both highly aromatic compounds, aromatic

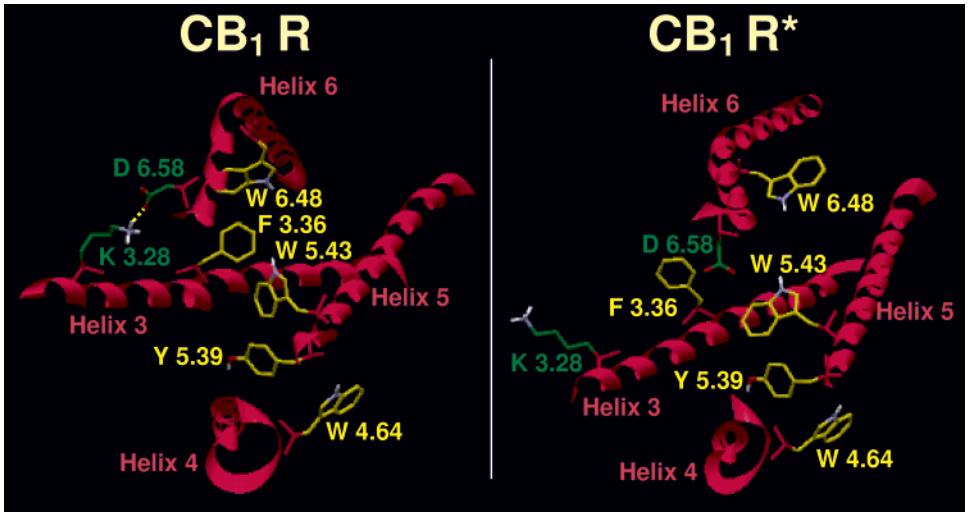

Figure 2. Models of the CB_1 R and R* states in the TMH3−4−5−6 region (in the absence of ligand) are illustrated here. (a) In the R state model, a salt bridge can form between K3.28 and D6.58 (shown in green). A microdomain of clustered aromatic residues (shown in yellow), W6.48/F3.36/W5.43/Y5.39/W4.64 exists in the CB_1 TMH3−4−5−6 region. (b) The conformational changes that occur upon receptor activation (R → R* transition) result in rotations of TMHs 3 and 6, as well as a change in the conformation of TMH6 (by moderation of its proline kink angle).[10−13] The K3.28−D6.58 salt bridge is broken (residues illustrated in green). The aromatic cluster present in the inactive state model also undergoes rearrangement, with W6.48/W5.43/Y5.39/W4.64 (shown in yellow) maintaining an extended cluster, while F3.36 (yellow) is no longer part of this cluster.

stacking interactions may be important to the affinity of each compound for the CB_1 receptor. Therefore, the goal of the work presented here was to identify through modeling studies those aromatic residues in the TMH3−4−5−6 aromatic microdomain of CB_1 that may contribute to WIN55,212−2 and SR141716A binding and then to experimentally test the results of these modeling studies through mutation. Modeling and mutation results reported here support the hypothesis that both SR141716A and WIN55,212−2 bind within the TMH3−4−5−6 aromatic microdomain region of CB_1. These results also reveal a divergence in the binding sites of anandamide and CP55,940 from those of SR141716A and WIN55,212−2.

Results

Comparison of R and R* State Models in the Absence of Ligand. The CB_1 R State. Figure 2a illustrates key features of the model of the CB_1 TMH bundle in the inactive (R) state in the TMH3−4−5−6 region. One of the significant features of the model of the CB_1 R TMH bundle is a salt bridge between K3.28(193) and D6.58(367) (N−O distance = 2.6 Å; N−H−O angle = 159°).[6] This salt bridge is made possible by the profound flexibility in TMH6 due to the presence of G6.49 in the CWXP motif of TMH6.[9] The TMH3−4−5−6 region of the R bundle in the absence of ligand is characterized by a W6.48(357)/F3.36(201)/W5.43(280)/Y5.39(276)/W4.64(256) aromatic cluster in which W6.48 stacks with F3.36 (d = 5.3 Å, α = 90°), while F3.36 stacks with W5.43 (d = 5.6 Å, α = 40°). W5.43 also has an off-set parallel stack with Y5.39 (d = 5.9 Å, α = 0°), while Y5.39 stacks with W4.64 (d = 6.5 Å, α = 90°) (see the Experimental Section for definitions of d and α).

The CB1 R* State. Figure 2b illustrates key features of the model CB_1 TMH bundle in the active (R*) state in the TMH3−4−5−6 region. The conformational changes that occur upon receptor activation result in rotations of TMHs 3 and 6, as well as a change in the conformation of TMH6 (by moderation of its proline kink angle).[10−13] In our models, both W6.48(357) and F3.36(201) undergo a change in their χ_1 values from R to R*. χ_1 in W6.48(357) changes from g+ to trans and χ_1 of F3.36(201) changes from trans to g+ (see the Experimental Section for the definition of χ_1). In the R* TMH bundle, the K3.28(193) and D6.58(367) salt bridge is broken (N−O distance = 16.8 Å) because TMHs 3 and 6 rotate (counterclockwise from extracellular view) during the R to R* transition (i.e. activation).[14,15] K3.28(193) has rotated away from D6.58(367) toward TMH7, and D6.58(367) has rotated toward the TMH5−6 interface and is raised higher above the ligand binding pocket due to the moderation of the TMH6 proline kink angle. The W6.48(357)/F3.36(201)/W5.43(280)/Y5.39(276)/W4.64(256) aromatic cluster present in the inactive state in the absence of ligand also undergoes rearrangement, with F3.36 no longer part of this cluster. In the TMH3−4−5−6 region of R* in the absence of ligand, W6.48 and W5.43 form an off-set parallel aromatic stacking interaction with each other (d = 4.9 Å, α = 30°). W5.43 also stacks with Y5.39 (d = 6.6 Å, α = 60°), while Y5.39 stacks with W4.64 (d = 5.7 Å, α = 90°). This series of aromatic stacking interactions results in a large aromatic stack in R* comprised of W6.48(357)/W5.43(280)/Y5.39(276)/W4.64(256). F3.36 (χ_1 = g+) is not located near an aromatic residue in the R* bundle; instead F3.36 is bounded by V3.40(205), V3.32(197), and L6.44(353).

Receptor Docking: Ligand Binding Sites. In the traditional two-state model for agonist action at GPCRs, a receptor is thought to exist in two states that are in equilibrium with each other, the ground or inactive (R) state and the active (R*) state.[16] The binding of an agonist ligand is thought to shift the equilibrium toward R*, resulting in an increase in GDP/GTP exchange, which initiates the signaling cascade. In the most widely discussed mechanism of inverse agonism, the inverse agonist preferentially binds to the R over R* state,[17] thus suppressing ligand-independent (constitutive) activation. Figures 3, 5, and 6 illustrate the binding sites

Table 1. Ligand−Aromatic Stacking Interactions in CB_1 R and R*

	SR141716A[a] in R				WIN55,212−2 in R*			
	MC[b]		DC[c]		NAP[d]		IND[e]	
	d[f] (Å)	α[g] (deg)	*d* (Å)	α (deg)	*d* (Å)	α (deg)	*d* (Å)	α (deg)
F3.36	7.9	NA[h]	**5.0**[i]	**80**	**6.4**	**20**	**6.3**	**50**
Y5.39	**6.5**	**25**	10.6	NA	10.7	NA	9.7	NA
W5.43	**4.8**	**50**	**4.8**	**90**	**4.5**	**90**	6.1	NA
W6.48	11.7	NA	7.6	NA	**4.2**	**60**	8.1	NA

[a] See ref 6. [b] MC = monochlorophenyl ring. [c] DC = dichlorophenyl ring. [d] NAP = naphthyl ring. [e] IND = indole ring system. [f] *d* = distance between aromatic ring centroids. [g] α = angle between normal vectors of interacting rings. [h] NA, intervening amino acid(s) prevent(s) a stacking interaction. [i] Distances (*d*) and angles (α) for aromatic systems that meet the criteria for aromatic stacking interactions[18] are highlighted in bold.

identified for the CB_1 inverse agonist SR141716A in the R state[6] and for the CB agonists WIN55,212−2 and anandamide, each in the R* state.

Aromatic stacking interactions were identified for both SR141716A and WIN55,212−2. Table 1 compares modeling results for SR141716A[6] with those for WIN55,-212−2. In this table, distances (*d*) and angles (α) for aromatic systems that meet the criteria for aromatic stacking interactions[18] are highlighted in bold.

SR141716A in the R State. SR141716A has been shown to act as a competitive antagonist and inverse agonist in host cells transfected with exogenous CB_1 receptor, as well as in biological preparations endogenously expressing CB_1.[19−21] The SR141716A-CB_1 interaction presented here focuses on the R state of CB_1.[6] SR141716A was found to have a single, direct aromatic stacking interaction with F3.36(201) and with Y5.39-(276) and two direct stacking interactions with W5.43-(280) in CB_1 R (Table 1). These direct interaction sites are colored yellow in Figure 3. The SR141716A/W5.43 interaction is the strongest, as W5.43 has aromatic stacking interactions with both the monochloro (MC) and dichlorophenyl (DC) rings of SR141716A. F3.36 has a single tilted-T aromatic stacking interaction with the DC ring of SR141716A at a close distance between ring centroids (5.0 Å), while the single aromatic stacking interaction of the MC ring of SR141716A with Y5.39 is weaker, because of the longer distance between ring centroids (6.0 Å). In binding, SR141716A becomes part of the aromatic cluster in the TMH3−4−5−6 region. In one of these clusters, F3.36(201) directly stacks with W6.48 (d = 4.9 Å, α = 50°) and with W5.43 (d = 5.9 Å, α = 60°). In a second cluster, Y5.39(276) directly stacks with W4.64 (d = 6.5 Å, α = 80°). Aromatic residues that are not direct interaction sites for SR141716A, but are part of this extended cluster, are illustrated in green in Figure 3.[6] F3.25(190) (colored blue in Figure 3) was not found to be part of this extended cluster. Modeling studies also suggested that in the SR141716A/CB_1 R complex, the carboxamide oxygen of SR141716A forms a hydrogen bond with K3.28 (N−O distance = 2.7 Å; O−H−N angle = 163°). We have recently shown using a mutant cycle that K3.28 is, in fact, a direct interaction site for the C-3 substituent of SR141716A.[6]

The docking position identified for SR141716A is consistent with SR141716A SAR results reported by Thomas and co-workers for substitution on the monochlorophenyl (MC) and dichlorophenyl (DC) rings.[22] Thomas reported that substitution at the 3 or 6 position on the DC ring with iodine resulted in a decrease in CB_1 affinity. In the SR141716A docked position reported here, substitution of an iodine at the 3 or 6 position on the DC ring would result in steric clashes with F3.36 for the 3 position and steric clashes with V6.56 and V6.59 for the 6 position (see Figure 4A). These substitutions would therefore be expected to reduce CB_1 affinity. Thomas also reported that substituent enlargement at the 4 position on the MC ring of SR141716A from chloro to bromo or iodo did not result in a significant loss of CB_1 affinity. Katoch-Rouse and co-workers reported that substitution of a methoxy group at the 4 position on the MC ring did not significantly affect CB_1 affinity as well.[23] In the SR141716A docked position reported here, substitution of bromo, iodo, or methoxy at the 4 position on the MC ring would not produce a steric clash, because this substituent resides in an area with adjacent unoccupied space (see Figure 4B).

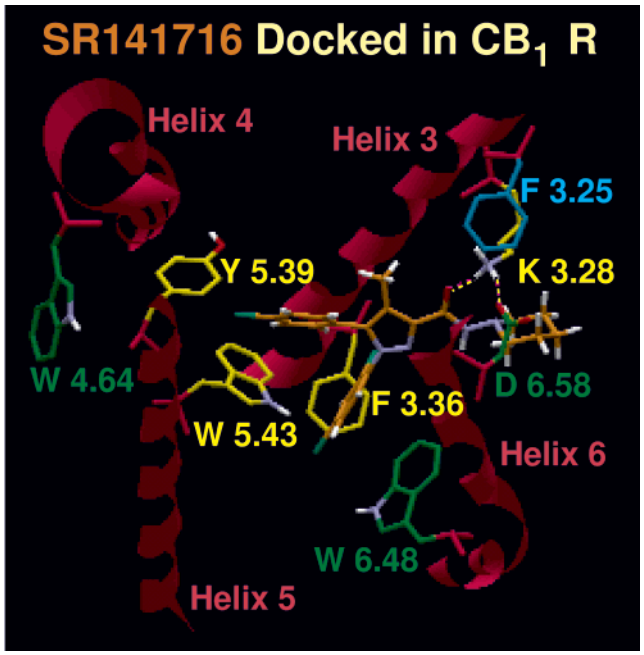

Figure 3. The model of the SR141716A/CB_1 R complex in the TMH3−4−5−6 region of CB_1 is illustrated here. SR141716A is in a minimum-energy conformation that produces the most negative electrostatic potential in the C3 substituent region. In this conformation (0.92 kcal/mol above the global minimum), the piperidine ring is in a chair conformation with the nitrogen lone pair of electrons pointing in the same direction as the carboxamide oxygen.[6] The carboxamide oxygen of SR141716A is involved in a hydrogen-bonding interaction with K3.28 (shown in yellow). K3.28 is also involved in a salt bridge with D6.58 (shown in green). Aromatic residues with which SR141716A stacks directly are shown in yellow. Aromatic residues with which SR141716A does not stack directly, but that are part of the extended aromatic cluster formed by SR141716A binding, are illustrated in green.

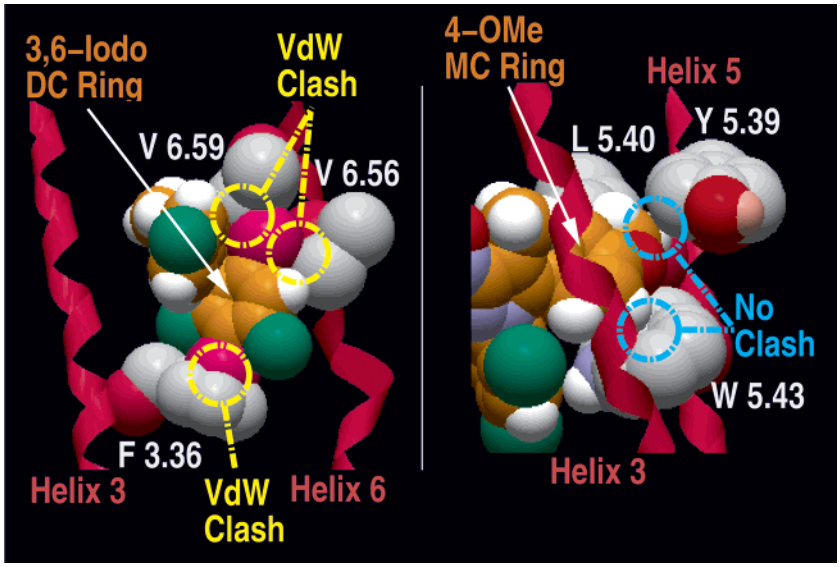

Figure 4. This figure illustrates the consistency of the SR141716A binding site model identified here with published SAR.[22,23] (A) SR141716A would have steric overlaps with CB_1 if an iodo substituent was located at the 3 or 6 position on the dichloro (DC) ring. (B) SR141716A would not have steric overlaps with CB_1 if a substituent as large as a methoxy were located at the 4 position on the monochloro (MC) ring.

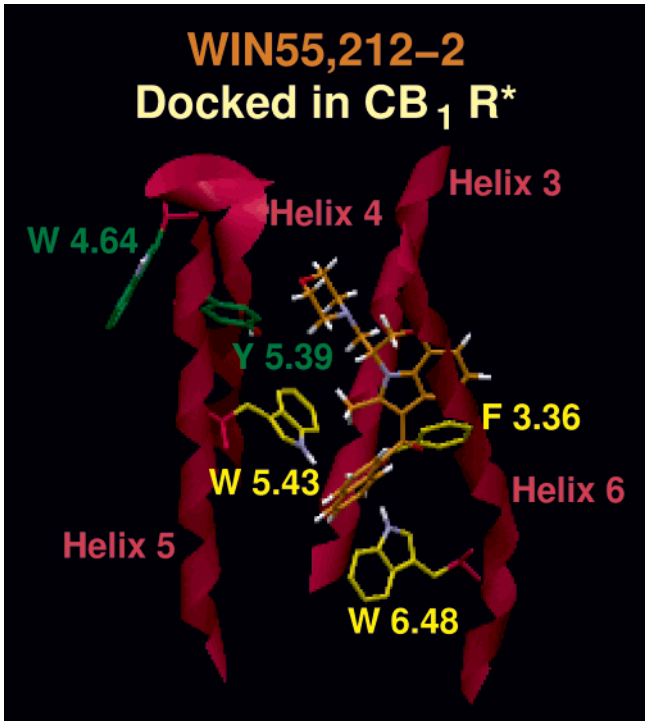

Figure 5. The model of the WIN55,212−2/R* complex in the TMH3−4−5−6 region of CB_1 is illustrated here. WIN55,212−2 was docked in its lowest energy s-trans conformation.[45] Aromatic residues with which WIN55,212−2 stacks directly are shown in yellow. Aromatic residues with which WIN55,-212−2 does not stack directly, but that are part of the extended aromatic cluster formed by WIN55,212−2 binding, are illustrated in green.

WIN55,212−2 in the R* State. Figure 5 and Table 1 illustrate modeling results for the CB agonist WIN55,-212−2 in the CB_1 R* state. WIN55,212−2 was docked in a model of the CB_1 active (R*) state, because agonists are thought to have higher affinity for the R* form of a GPCR versus the R form. In our CB_1 model, the R → R* transition results in the loss of direct interactions between W5.43(280), F3.36(201), and W6.48(357). In the model, this triad is once again linked with each other via WIN55,212−2, which bridges the gap between these residues in the ligand/R* complex. WIN55,212−2 has a direct aromatic stacking interaction with W5.43(280) and W6.48(357) and two direct stacking interactions with F3.36(201). The distances (d) and angles (α) for these interactions are given in bold in Table 1, and residues with which WIN55,212−2 interacts directly are illustrated in yellow in Figure 5. Aromatic residues in the TMH3−4−5−6 region form a network or cluster with which WIN55,212−2 interacts. W5.43(280) directly stacks with Y5.39 (d = 6.1 Å, α = 60°), and Y5.39(276) stacks with W4.64 (d = 5.3 Å, α = 70°). In binding, WIN55,212−2 becomes part of an aromatic cluster that includes F3.36(201)/W6.48(357)/W5.43(280)/Y5.39(276)/W4.64(256) in the minimized complex. No hydrogen-bonding interactions were identified for WIN55,212−2 in CB_1 R*. This result is consistent with recent reports by Huffman and co-workers that cannabimimetic indoles retain high CB_1 affinity even when all hydrogen-bonding potential has been removed (see compound **26** in ref 46).

The binding site identified here for WIN55,212−2 is consistent with AAI SAR data that demonstrated that the *R* stereoisomer of WIN55,212 (called WIN55,212−2), but not the *S* stereoisomer of WIN55,212 (called WIN55,212−3), produced effects at the cannabinoid receptor.[24] In the docking position illustrated for WIN55,-212−2 here, WIN55,212−3 would not be able to fit because the morpholino alkyl tail would be sterically blocked by the TMH6 backbone and residues V6.59(368) and M6.55(364). Early results reported by D'Ambra and co-workers[24] for WIN55,212 (a mix of R + S isomers, C-2 Me) and its C-2 H and C-2 Et congeners showed that when the C-2 substituent was a hydrogen atom or a methyl group, compounds with good CB_1 affinity and efficacy were produced. However, the analogue in which the C-2 substituent was an ethyl group was essentially an inactive compound. Our docking studies indicated that if the C-2 substituent was enlarged from methyl

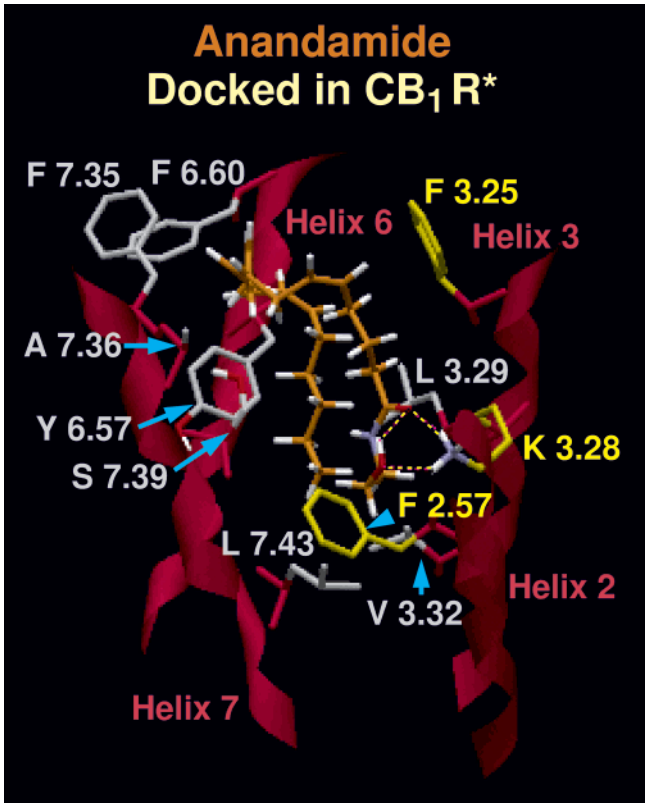

Figure 6. The anandamide/R* complex in the TMH2−3−6−7 region of CB_1 R* is illustrated here. K3.28(193) forms a hydrogen bond with the amide oxygen of anandamide. At the same time, the headgroup hydroxyl of anandamide is engaged in an intramolecular hydrogen bond with its amide oxygen. The anandamide binding pocket is lined with residues (shown in gray) that are largely hydrophobic, including L3.29, V3.32, F6.60, F7.35, A7.36, Y6.57, S7.39 (hydrogen bonded back to its own backbone carbonyl oxygen), and L7.43. F3.25 (shown in yellow) has a C−H···π interaction with the C5−C6 double bond of anandamide, while F2.57 (shown in yellow) has an interaction with the amide oxygen of anandamide.

to ethyl, the naphthyl ring would have to adjust its tilt and make the ring more perpendicular to the plane of the indole due to steric constraints. This adjustment, however, results in a steric clash with W5.43(280) in the receptor binding pocket, such that the ligand has to back away from the aromatic cluster, losing most of the aromatic stacking interactions illustrated in Figure 5 for WIN55,212−2.

Anandamide in R*. While anandamide is not capable of engaging in aromatic ($\pi-\pi$) stacking interactions, it can engage in C−H···π interactions. Figure 6 illustrates results of docking studies for the endogenous agonist anandamide in CB_1 R*. Anandamide was employed in this study as a control, since a docking study of several dimethylanandamides[25] suggested that the TMH2−3−7 region, not the TMH3−4−5−6 aromatic residue rich region of CB_1, was the binding site. Docking studies reported here suggest that in its binding site in the CB_1 TMH2−3−6−7 region, anandamide is engaged in a hydrogen-bonding interaction with K3.28(193). In this interaction, K3.28(193) forms a hydrogen bond with the amide oxygen of anandamide (N to amide O distance = 2.6 Å, N−H−O angle = 158°). At the same time, the headgroup hydroxyl of anandamide is engaged in an intramolecular hydrogen bond with the amide oxygen (O to O distance = 2.7 Å O−H−O angle = 130°). The formation of such an intramolecular hydrogen bond in anandamide helps the hydroxyl exist in a hydrophobic region and still satisfies a hydrogen bond.

The residues that line the anandamide binding pocket are largely hydrophobic, including F2.57(171), F3.25(190), L3.29(194), V3.32(197), F6.60(369), F7.35(380), A7.36(381), Y6.57(366), S7.39(384) (hydrogen bonded back to its own backbone carbonyl oxygen), and L7.43(388). The interaction with F3.25(190) is a C−H···π interaction with the C5−C6 double bond in anandamide. In the R* bundle, F2.57(171) has an interaction with the amide oxygen. Here, an aromatic ring hydrogen interacts with one of the lone pairs of electrons of the amide oxygen (C−O distance = 3.7 Å, C−H−O angle = 168°, ring center to O distance = 5.1 Å). A similar interaction is evident in the X-ray structure of bovine rhodopsin[26] in which F5.38(203) points its positive edge into the backbone carbonyl oxygen of P4.60 (C−O distance = 3.3 Å, C−H−O = 147°, ring center to O distance = 4.6 Å).

We have previously shown that the arrangement of homoallylic double bonds in the acyl chain portion of anandamide makes anandamide a very flexible molecule.[25,27] While there are no crystal structures of anandamide bound to CB_1 available in the literature, there is an X-ray crystal structure of anandamide's parent acid, arachidonic acid (20:4, $n-6$), complexed with adipocyte lipid binding protein.[28] In this structure, arachidonic acid clearly adopts a curved/U-shaped conformation that is consistent with the conformations identified for anandamide (20:4, $n-6$) in our conformational memories calculations[25,27] and is consistent with the conformation of anandamide in CB_1 illustrated in Figure 6. The importance of K3.28(193) as a direct interaction site for anandamide is supported by the work of Song and Bonner,[29] who reported that anandamide was unable to compete for [^{3}H]WIN55,212−2 binding in a human CB_1 K3.28(192)A mutant and that the potency of anandamide in inhibiting cAMP accumulation was reduced >100-fold in this mutant. This loss of affinity could occur with the loss of a strong hydrogen-bonding interaction.

The binding-site interactions illustrated for anandamide in Figure 6 agree with results first reported by Pinto and co-workers,[30] which showed that the hydroxyl group in the headgroup region of anandamide could be replaced by a methyl group without a loss in CB_1 affinity. This result suggested that the hydroxyl group is *not essential* for anandamide binding and also that this hydroxyl may exist in a hydrophobic region of CB_1. This result has been echoed in later endocannabinoid structure−activity relationship studies that showed, for example, that a cyclopropyl headgroup results in a very high CB_1 affinity ligand.[31] In the binding site, identified for anandamide in our model, the headgroup hydroxyl is located in a hydrophobic pocket and satisfies its hydrogen-bonding potential by forming an intramolecular hydrogen bond with the amide oxygen. This result is consistent with recent NMR solution studies of anandamide reported by Bonechi and co-workers,[32] who found that this intramolecular hydrogen bond in anandamide persists in solution.

We recently reported that the TMH2−3−7 region of CB_1 was the binding site for a series of dimethylanand-

Table 2. Cannabinoid Receptor Radioligand Binding Determinations in Membranes Prepared from Wild Type and Mutant Cell Lines[a]

cell line	K_d (nM)	B_{max} (pmol/mg)
WT CB_1	1.5 (0.53−2.4)	4.4 (3.5−5.3)
F3.25(190)A	5.5 (0.3−10)	3.2 (1.9−4.5)
F3.36(201)A	2.3 (0.6−4.1)	5.2 (3.6−6.9)
W4.64(256)A	ND	ND
W5.43(280)A	5.4 (1.2−9.5)	1.9*(1.1−2.6)
W6.48(357)A	3.2 (2.0−4.4)	4.4 (3.8−5.2)

[a] Experiments using [^{3}H]CP55,940 were performed on stably transfected HEK 293 cells to evaluate binding affinities and relative levels of receptor expression in the wild-type and mutant receptors. Nonspecific binding was determined in the presence of excess CP55,940 (see Experimental section). Data are the means and corresponding 95% confidence limits of three independent experiments each performed in triplicate. The asterisk (*) indicates statistically significant differences from wild type ($p < 0.05$). ND, not determined.

amide analogues.[25] Results of docking studies here indicate that anandamide can occupy a slightly different position in CB_1 (the TMH2−3−6−7 region) due to the absence of the two methyl groups at C2 and C1′ found in the dimethylanandamide analogues previously studied.

CP55,940 in CB1 R*. CP55,940 is used here as the radioligand for binding studies because its binding site does not involve interaction with the residues of the aromatic microdomain studied here. In our revised CB_1 model based upon the rhodopsin crystal structure,[26] CP55,940 binds higher up in the CB_1 R* binding pocket, above F3.36, W5.43, and W6.48 and to the side of F3.25 (ref 33 and manuscript in preparation). This CP55,940 binding site is extracellular to the binding site identified for WIN55,212−2 and involves hydrogen-bonding interactions of the southern aliphatic hydroxyl (SAH) of CP55940 with K3.28, the northern aliphatic hydroxyl of CP55940 (NAH) with K260 in the CB_1 EC-2 loop, and the phenolic hydroxyl of CP55940 with D6.58.

Receptor Recognition of Cannabinoid Ligands. To test the binding-site hypotheses generated by the receptor model, selective mutations of aromatic residues in TMHs 3, 4, 5, and 6 of the CB_1 receptor were generated and stable cell lines were established. Stable cell lines were created in HEK-293 cells expressing either mouse wild-type CB_1 (WT CB_1), F3.25(190)A, F3.36(201)A, Y4.64(256)A, W5.43(280)A, or W6.48-(357)A, and Scatchard analyses were performed using [^{3}H]CP55,940 as the radioligand (Table 2). No specific [^{3}H]CP55,940 binding to HEK 293 cells was found prior to transfection (data not shown). The affinity values obtained for all the mutant receptors were not significantly different from WT CB_1 receptor (Table 2). These results are in agreement with the receptor model that predicted the aromatic residues chosen for mutational analysis would not be interaction sites for the bicyclic cannabinoid, CP55,940 (see above). Since significant changes in the affinity of [^{3}H]CP55,940 were not observed, this tritiated compound served as an excellent tool for ligand competition studies. The mutation of human W4.64A has been previously reported to result in receptor sequestration in a mammalian cell line.[3] In agreement with this previous finding, we found that mouse W4.64(256)A was not properly expressed on the cell surface in HEK cells as assessed by immunofluorescence (Figure 7). Compared to WT CB_1, few cells showed surface expression of the mutant protein. We also tested this mutation in an amphibian cell (oocyte) background versus a mammalian to determine if *Xenopus* oocytes might process the mutant protein correctly, but functional expression was not observed (data not shown). Further characterization of W4.64(256)A was not carried out because of these findings. These results for the W4.64A mutant are similar to those reported by Rhee and co-workers for the W4.64A mutation in CB_2, which exhibited no binding of any ligand, suggesting improper folding or lack of cell surface expression.[34]

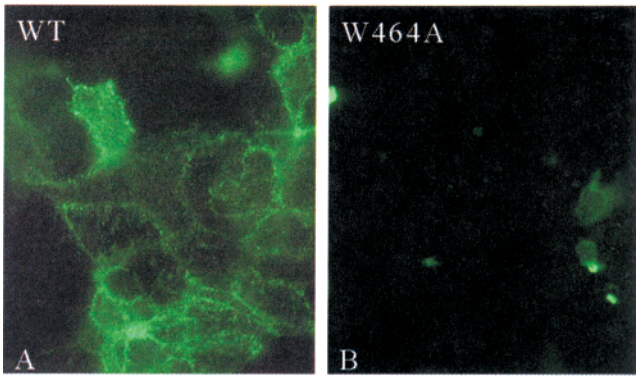

Figure 7. Immunolabeling of HEK 293 cells stably expressing wild type (WT) CB_1 receptor (A) or transiently expressing W4.64A mutant CB_1 receptor (B). Bright cell surface labeling was observed around cells expressing the wild-type CB_1 receptor. The majority of cells that were transfected with the W4.64A mutant CB_1 receptor did not express the protein on their cell surface.

Table 3. Ability of Three Cannabinoid Receptor Ligands to Displace [^{3}H]CP55,940 from Membranes Prepared from Wild Type and Mutant Cell Lines[a]

	K_i		
cell line	WIN55,212−2[b]	anandamide[c]	SR141716A[b]
WT CB_1	12 (7.0−20)	0.3 (0.1−0.6)	4.8 (2.2−10)
F3.25(190)A	15 (3.7−49)	1.8* (0.6−5.6)	9.6 (4.6−20)
F3.36(201)A	107*(44−261)	0.3 (0.1−1.1)	14* (7.3−29)
W4.64(256)A	ND	ND	ND
W5.43(280)A	199* (43−914)	0.3 (0.2−0.7)	46%* displacement at 5 μM
W6.48(357)A	45* (22−92)	0.3 (0.1−0.5)	33* (23−45)

[a] Inhibition constants were obtained from competition experiments (see Experimental section). Data are the means and corresponding 95% confidence limits of three independent experiments each performed in triplicate. The asterisk (*) indicates statistically significant differences from wild type ($p < 0.05$). ND, not determined. [b] In nM. [c] In μM.

Ligand Displacement Studies. F3.25(190)A Receptor Affinity. The F3.25(190)A mutation had no statistically significant effect on WIN55,212−2 or SR141716A binding, but it resulted in a 6-fold loss in affinity for anandamide (Table 3, Figure 8). This result is consistent with modeling studies (see Figures 3, 5, and 6) that show that F3.25(190) is not part of the binding site of WIN55,212−2 (in R*) or SR141716A (in R) but is a part of the anandamide binding pocket (in R*).

F3.36(201)A Receptor Affinity. The affinity of anandamide was unaffected by the F3.36(201)A mutation, whereas the affinities of both WIN55,212−2 (9-fold loss) and SR141716A (3-fold loss) were affected by this mutation (Table 3, Figure 8). The binding results for anandamide are consistent with the modeling stud-

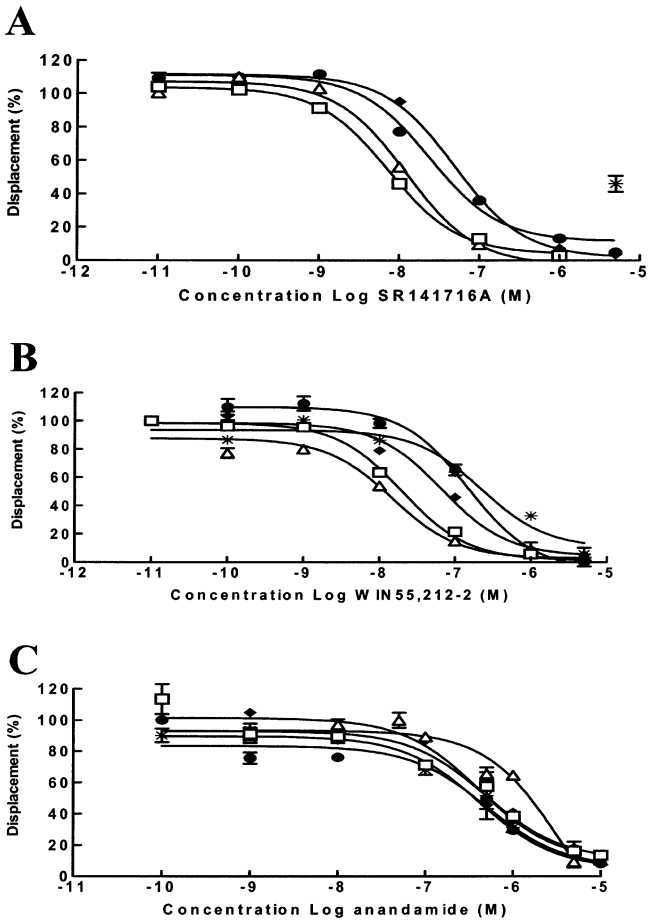

Figure 8. Displacement of [^{3}H]CP55,940 by SR141716A (A), WIN55,212−2 (B), or anandamide (C) in membranes prepared from HEK 293 cells transfected with wild-type or mutant CB_1 receptors. Displacement curves were obtained in stable cell lines expressing [□] WT CB_1, [△] F3.25(190)A, [●] F3.36(201)A, [*] W5.43(280)A, and [◆] W6.48(357)A. Each data point shown is the mean ± SE of at least three independent experiments performed in triplicate.

ies that did not identify F3.36 as a direct interaction site for anandamide. Results for WIN55,212−2 and SR141716A are consistent with receptor docking studies reported above, which show that F3.36(201) is a direct interaction site for both WIN55,212−2 (in R*) and SR141716A (in R). As illustrated in Figure 5, F3.36-(201) forms two stacking interactions with WIN55,212−2, as this residue can interact with both the naphthyl (NAP) and the indole (IND) rings of WIN55,212−2. Figure 3 illustrates that F3.36(201) has a single aromatic stacking interaction with the dichlorophenyl (DC) ring of SR141716A in the R state of WT CB_1. It is likely that SR141716A can partially compensate for the loss of aromaticity at 3.36(201) in the F3.36(201)A mutant through a strengthened aromatic stacking interaction with W6.48(357), which is located just beneath F3.36-(201) in the WT CB_1 R state (Figure 3).

W5.43(280)A Receptor Affinity. The W5.43(280)A mutation produced an 8-fold loss in affinity for WIN55,-212−2, but it did not affect anandamide binding (Table 3, Figure 8). This result is consistent with the modeling studies that suggest that W5.43(280) is not part of the anandamide binding pocket but suggest that WIN55,-212−2 has a direct aromatic stacking interaction between W5.43(280) and its NAP ring. This aromatic stacking interaction can be expected to be particularly strong as the centroid to centroid distances between interacting rings is at close distance (4.5 Å) and the angle of the interacting ring planes is 90°, forming a perfect tilted-T arrangement (see Table 1).[18]

The W5.43(280)A mutation had the most profound effect on SR141716A binding compared to any of the mutations reported here. Even at 5 μM, SR141716A could only displace 46% of tritiated CP55,940. The nonspecific effects of cannabinoids produced beyond 5 μM precluded us from testing higher concentrations. This result is consistent with the modeling studies that suggested that W5.43(280) is central in the aromatic cluster interactions with SR141716A. As detailed in Table 1 and illustrated in Figure 3, the model suggests that W5.43 has direct stacking interactions with both the MC and DC rings of SR141716A. It is likely that W5.43 helps orient SR141716A in the binding pocket, so loss of aromaticity at W5.43(280) would be expected to have a particularly deleterious effect upon SR141716A binding.

W6.48(357)A Receptor Affinity. The binding of anandamide was unaffected by the W6.48(357)A mutation, whereas the binding of both WIN55,212−2 (4-fold loss) and SR141716A (7-fold loss) was affected by this mutation (Table 3, Figure 8). These results are also consistent with modeling results for anandamide, which suggest that W6.48(357) is not part of the anandamide binding site, and with results for WIN55,212−2, which suggest a direct stacking interaction between W6.48-(357) and the NAP ring of WIN55,212−2. The magnitude of the effect of the W6.48(357)A mutation on SR141716A binding (7-fold loss) was, however, more than would be expected from a cursory inspection of the modeling study illustrated in Figure 3, as W6.48(357) does not stack directly with SR141716A but stacks with F3.36(201), which, in turn, stacks with SR141716A. It is possible that the decrease in affinity upon mutation of W6.48 to alanine is due to the loss of the extended aromatic stacking interaction between SR141716A, F3.36, and W6.48, as only one stacking interaction would remain (i.e. between SR141716A and F3.36).

Discussion

In the absence of a crystal structure for CB_1, the combination of site-directed mutagenesis and molecular modeling is a powerful tool that allows us to study specific ligand−receptor interactions. In this study, we wanted to determine if aromatic residues in the binding pocket of CB_1 form specific interaction sites for aminoalkylindole agonist (WIN55,212−2) and diaryl pyrazole inverse agonist/antagonist (SR141716A) ligands, but not for endogenous (anandamide) and nonclassical cannabinoid (CP55,940) agonists.

Importance of CB1 TMH3−4−5−6 Region. Mutation results reported here in Table 3 suggest that TMH3−4−5−6 aromatic microdomain residues F3.36, W5.43, and W6.48 are part of the binding pocket for both SR141716A and WIN55,212−2. One important proviso associated with any mutation study is the possibility that a gross structural change has occurred in the ligand binding pocket as the result of a mutation. In this case, it is possible that a change in a residue distant from the ligand binding pocket could have an effect on ligand

binding. Such a structural change is unlikely here for three reasons: (1) the amino acid residue chosen as the replacement is smaller than the WT residue, as recommended by Ward et al.,[35] (2) the replacement residue is not a helix breaker, such as Pro or Gly,[36] and is not a residue that has been documented to induce helix bends, such as Ser or Thr,[37] and (3) both CP55,940 and anandamide retain WT affinity for the F3.36A, W5.43A, and W6.48A mutants, providing strong evidence that a structural rearrangement in the binding pocket has not occurred here.[35]

The identification of the TMH3−4−5−6 region as the binding region of SR141716A and WIN55,212−2 is supported by previous mutation/chimera studies. A recent CB_1 mutant cycle study indicated that K3.28 is a direct interaction site for the C-3 substituent of SR141716A.[6] Shire and co-workers have shown in CB_1/CB_2 chimera studies that the TMH4-E2-TMH5 region of CB_1 contains residues critical for the binding of SR141716A and WIN55,212−2.[3] Mutation studies performed by Song and co-workers have supported the importance of the TMH3−4−5 region of CB_1 and CB_2 for the binding of WIN55,212−2.[5] These studies showed that the 15−20-fold higher affinity of WIN 55,212−2 for the CB_2 receptor may be due in part to a direct aromatic stacking interaction with F5.46, a residue that is aromatic only in CB_2.

Aromatic ($\pi-\pi$) Stacking Interactions in CB_1 Ligand Recognition. Another hypothesis tested here is that aromatic stacking interactions are important for the binding of aminoalkylindole agonists (such as WIN55,212−2) and diaryl pyrazole inverse agonist/antagonists (such as SR141716A) at CB_1. Attractive $\pi-\pi$ interactions are one of the major noncovalent forces governing molecular recognition. Burley and Petsko[18] have reported that aromatic−aromatic stacking interactions in proteins operate at distances (d) of 4.5−7.0 Å between ring centroids. The angle (α) between normal vectors of interacting aromatic rings typically is between 30° and 90°, producing a "tilted-T" or "edge-to-face" arrangement of interacting rings. Hunter and co-workers[38] have reported that $\pi-\pi$ parallel stacking interactions ($\alpha < 30°$) between phenylalanine residues in proteins are also favorable if the rings are offset from each other. Recent ab initio calculations on benzene dimers have estimated that tilted-T and off-set parallel $\pi-\pi$ (aromatic) stacking interactions have stabilization energies of 2.7 and 2.8 kcal/mol respectively, suggesting that these may be very important noncovalent interactions.[39]

In addition to W4.64 and Y5.39, docking studies reported here identified F3.36, W5.43, and W6.48 as part of the binding pockets of SR141716A and WIN55,212−2 (Table 1, Figures 3 and 5). These docking results suggest that aromatic stacking interactions may be important for AAI and diaryl pyrazole ligand binding. Consistent with the docking results, we have reported here that mutation of F3.36, W5.43, or W6.48 to a nonaromatic residue (alanine) results in reduced affinity for SR141716A and WIN55,212−2. If such an affinity decrease is the direct result of loss of aromatic stacking interactions via substitution of a nonaromatic for an aromatic residue within the ligand binding pocket, then a comparable change in the ligand should also lead to a decrease in affinity, i.e., in each ligand structural class, substitution of nonaromatic for aromatic moieties of equivalent or smaller size (with no change in the receptor binding site) should also result in reduced receptor affinity. Consistent with this premise, SAR studies of the C-5 substituent of SR141716A (monochlorophenyl (MC) ring) have indicated that loss of aromaticity in the C5 substituent results in ligands with dramatically reduced CB_1 affinities.[40,41] Loss of aromaticity in the N1 substituent of SR141716A (the dichlorophenyl (DC) ring) by a change to a cyclohexyl N1 substituent has been reported to result in a significant loss in CB_1 affinity as well.[42]

The importance of aromaticity for proper AAI interaction with CB_1 has been illustrated by Huffman and co-workers.[43] These investigators reported that replacement of the naphthyl (NAP) ring of WIN55,212−2 with an alkyl (CH_3) or alkenyl [$(CH_3)_2C{=}CH$] group resulted in complete loss of CB_1 affinity (K_i > 10 000 nM) in both cases. Eissenstat and co-workers[44] reported that replacement of the naphthyl ring of WIN55,212−2 with a hydrogen resulted in a compound with a very high IC_{50} at CB_1. These findings are significant because they underscore that an aromatic system as part of the C-3 substituent of WIN55,212−2 may be important and because it suggests that the requirement at this position is not simply a requirement for any hydrophobic moiety.

While recent CB_1 K3.28A mutation studies[6] have indicated that SR141716A binding to CB_1 involves a hydrogen bond between the C-3 substituent of SR141716A and K3.28 (see Figure 3), hydrogen bonding does not appear to be important for WIN55,212−2 interaction with CB_1. Song and Bonner reported that a CB_1 K3.28A mutation had no effect on the affinity of WIN55,212−2 for CB_1.[29] The carbonyl oxygen of WIN55,212−2 would appear to be a likely hydrogen-bond acceptor; however, rigid AAI analogues in which the carbonyl group was replaced with a methylene group, the E naphthylidene indenes, have been shown to retain high affinity at both the CB_1 and CB_2 receptors.[45] Huffman and co-workers[46] recently synthesized an indole analogue of WIN55,212−2 for which all hydrogen-bonding potential was removed. This compound was found to retain high CB_1 affinity. These results support the modeling reported here that indicates that hydrogen bonding is not important for interaction of the AAI WIN55,212−2 with CB_1.

C−H$\cdots\pi$ Interactions in CB1/Endocannabinoid Recognition. C−H$\cdots\pi$ interactions are moderate, but nevertheless important, interactions that contribute to protein stability.[47] Mutation studies reported here suggest that F3.25 is part of the binding site of anandamide, while modeling studies suggest that F3.25 has a C−H$\cdots\pi$ interaction with the C5−C6 bond of anandamide. This interaction is consistent with the recent crystal structure of fatty acid amide hydrolase (FAAH) in which the arachidonyl inhibitor methoxy arachidonyl phosphonate (MAP) is bound.[48] Here several aromatic amino acids (F194, F244, Y335, F381, F432, and W531) line the substrate binding pocket surrounding the arachidonyl chain and F194, F381, and F432 are engaged in C−H$\cdots\pi$ interactions with the first through third double bonds, respectively, of the MAP arachidonyl acyl chain. Binding-site interactions identified here for

anandamide also agree with the recent crystal structure of arachidonic acid bound to prostaglandin synthase.[49] This crystal structure shows C−H···π interactions between arachidonic acid acyl chain double bonds and aromatic residues.

Conclusions

Modeling and mutation studies reported here suggest that the aromatic microdomain in the TMH3−4−5−6 region comprised of F3.36, W4.64, Y5.39, W5.43, and W6.48 is the binding-site region for both SR141716A and WIN55,212−2, but not for anandamide. Only F3.25 was found to be important for the binding of anandamide at CB_1. These results indicate that the endocannabinoid binding pocket at CB_1 may only partially overlap the binding pockets of SR141716A and WIN55,-212−2.

Results reported here also suggest that the set of key noncovalent forces governing molecular recognition of the aminoalkylindoles (WIN55,212−2), diaryl pyrazoles (SR141716A), and the endocannabinoids (anandamide) at CB_1 may be different. For the antagonist/inverse agonist, SR141716A, a combination of aromatic stacking interactions and hydrogen bonding[6] are key, while aromatic stacking interactions alone appear to be the principal intermolecular forces governing the binding of the aminoalkylindole WIN55,212−2 at CB_1. For the endocannabinoid anandamide, C−H···π and hydrogen-bonding interactions appear to be key intermolecular forces for CB_1 recognition.

Experimental Section

Receptor Model Construction. Amino Acid Numbering System. In the discussion of receptor residues that follows, the amino acid numbering scheme proposed by Ballesteros and Weinstein[50] is used. In this numbering system, the most highly conserved residue in each transmembrane helix (TMH) is assigned a locant of 0.50. This number is preceded by the TMH number and followed in parentheses by the sequence number. All other residues in a TMH are numbered relative to this residue. In this numbering system, for example, the most highly conserved residue in TMH2 of the mouse CB_1 receptor is D2.50(164). The residue that immediately precedes it is A2.49(163). Figure 1 serves as a reference for this numbering system in CB_1.

Definition of the Rotameric State of χ1. Different nomenclatures have been used to define the rotameric state of side chain torsion angles. The nomenclature employed here for the χ1 (chi 1) torsion angle is that described by Shi and co-workers.[8] When the heavy atom at the γ position is at a position opposite to the backbone nitrogen when viewed from the β-carbon to the α-carbon, the χ1 is defined to be trans. When the heavy atom at the γ position is at a position opposite to the backbone carbon when viewed from the β-carbon to the α-carbon, the χ1 is defined to be gauche+ (g+). When the heavy atom at the γ position is at a position opposite to the α-hydrogen when viewed from the β-carbon to the α-carbon, the χ1 is defined to be gauche− (g−). Using this nomenclature system, the side chain conformations were categorized into g− (0° < χ1 < 120 °), trans (120° < χ1 < 240°), or g+ (240° < χ1 < 360°).

R to R* Transition in GPCRs. Because agonists are thought to have higher affinity for the activated form of GPCRs,[16] agonist ligands in the work reported here were docked in a model of the activated state (R*) of CB_1 (see below). This R* CB_1 model was created by modification of our rhodopsin (Rho)-based model of the inactive (R) form of CB_1 (see below) and guided by the biophysical literature on the R to R* transition. It has now been well-established in the Biophysical literature that the R to R* transition in GPCRs is accompanied by significant changes in the transmembrane helix bundle (see refs 15 and 36 for reviews). These studies have indicated that activation of Rho is accompanied by a rigid domain motion of TMH6 relative to TMH3.[10] Javitch and co-workers[14] documented that Cys 6.47 becomes available to the binding pocket only in a constitutively active β-2 mutant. The acquired accessibility of Cys 6.47 in the mutant was hypothesized to result from a counterclockwise rotation (from an extracellular view) and/or tilting of the sixth membrane spanning segment associated with activation of the receptor. Lin and Sakmar[51] reported that perturbations in the environment of W3.41 (along with W6.48) of Rho occur during the conformational change concomitant with receptor activation. W3.41(126) faces lipid in the inactive state of Rho.[26] Lin and Sakmar[51] attributed the observed differential shift of the Lb absorption of the indole side chain of Trp126(W3.41) in Rho during activation to the decreased hydrophobicity of its environment. This has been interpreted as originating from a counterclockwise rotation of TMH3 (from an extracellular view),[15] which would move this residue into the more polar environment of the TMH3-TMH4 interface. A ∼20° rotation of TMH3 would be required to rotate this residue in the Rho crystal structure out of lipid and into the TMH3−TMH4 interface.

Jensen and co-workers[13] recently demonstrated through fluorescence studies of the β-2-adrenergic receptor that P6.50 in the highly conserved CWXP motif of TMH6 can act as a flexible hinge that mediates the transition from R to R*. In the R state, these investigators propose that TMH6 is kinked at P6.50 such that its cytoplasmic end is nearly perpendicular to the membrane and close to the cytoplasmic end of TMH3. The transition to the R* state is accomplished by the straightening of TMH6 such that the cytoplasmic part of TMH6 moves away from the receptor core and upward toward the lipid bilayer.[13] Ballesteros and co-workers[52] recently proposed that a salt bridge between R3.50 and E6.30 at the intracellular end of the β-2-adrenergic receptor stabilizes this receptor in its inactive state.

In the present study, the literature on GPCR activation discussed above was used to generate an R* CB_1 TMH bundle from a model of the inactive (R) CB_1 receptor based on the 2.8 Å crystal structure of rhodopsin.[26] The creation of these two forms of CB_1 is described below.

Model of Inactive State (R) Form of CB_1. A model of the R form of CB_1 was created using the 2.8 Å crystal structure of bovine Rho.[26] First, the sequence of the mouse CB_1 receptor[53] (see Figure 1) was aligned with the sequence of bovine Rho using the same highly conserved residues as alignment guides that were used initially to generate our first model of CB_1.[54] TMH5 in CB_1 lacks the highly conserved proline in TMH5 of Rho. Therefore, the sequence of CB_1 in the TMH5 region was aligned with that of Rho as described previously using its hydrophobicity profile.[54] The mouse CB_1 sequence[53] is 97.7% identical to the human CB_1 sequence[55] overall and 100% identical within the transmembrane regions. The mouse sequence is one residue longer (473 residues) than the human sequence (472 residues) due to an additional residue in the N terminus.

Initial helix ends for mouse CB_1 were chosen in analogy with those of Rho:[26] TMH1, N1.28(113)−R1.61(146); TMH2, R2.37-(151)−H2.68(182); TMH3, S3.21(186)−R3.56(221); TMH4, T4.38(230)−C4.66(258); TMH5, H5.34(271)−K5.64(301); TMH6, R6.28(337)−K6.62(371); TMH7, K7.32(377)−S7.57(402); intracellular extension of TMH7, D7.59(404)−C7.71(416). With the exception of TMH1, these helix ends were found to be within one turn of the helix ends originally calculated by us and reported in 1995.[54] Two changes dictated by the CB_1 sequence were made in the helix ends. The shortness of the E1 loop region in CB_1 necessitated starting TMH3 at 3.23 [N3.23(188)−R3.56(221)]. The break in helicity caused by the GWNC sequence motif on the extracellular end of TMH4 necessitated that TMH4 end at 4.62 instead of 4.66 (as is found in Rho). Changes to the general Rho structure that were

necessitated by sequence divergences included the absence of helix-kinking proline residues in TMH1 and TMH5, the lack of a GG motif in TMH2, as well as, the presence of extra flexibility in TMH6.[9]

Because TMH6 figures prominently in the R to R* transition,[13] we have studied the conformations accessible to TMH6 in CB_1 and CB_2 using conformational memories (CM).[9] These studies revealed that TMH6 in CB_1 (but not CB_2) has high flexibility due to the small size of residue 6.49 (a glycine) immediately preceding Pro 6.50. Two families of conformers were identified by CM for TMH6 in CB_1. Cluster 1 showed a pronounced proline kink (40 members out of 100, 71.2° average kink angle). Cluster 2 contained helices with less pronounced kinks (51 members out of 100, 30.1° average kink angle). A conformer from the more kinked CM family of CB_1 TMH6s (cluster 1) was used in our model of the R state of CB_1. This conformer was selected (Pro kink angle = 53.1°) so that R3.50(215) and D6.30(339) could form a salt bridge at the intracellular ends of TMHs 3 and 6 in the CB_1 TMH bundle. An analogous salt bridge has been shown to be an important stabilizer of the inactive state of the β_2 adrenergic receptor[52] and to be present in Rho.[26] Because of the extreme flexibility of TMH6 in CB_1, we have proposed that an additional TMH3−6 salt bridge, K3.28(193)−D6.58(367), stabilizes the inactive state on the extracellular side of the TMH bundle.[6]

Model of Active (R*) Form of CB_1. On the basis of experimental results for rhodopsin and the β-2-adrenergic receptor,[10,13,14,51,52] the R* (active) CB_1 bundle was created from the inactive (R) model of CB_1 by rotating TMH3 so that residue 3.41 moves into the less hydrophobic environment of the TMH3−4 interface.[51] This was accomplished by a 20° counterclockwise (extracellular view) rotation of TMH3 from its orientation in the inactive (R) bundle. In the R* bundle, a TMH6 conformer from the second major conformational family (less kinked: 21.8° kink angle) identified by CM[9] was substituted for the TMH6 conformer used in the inactive model of CB_1. This conformer was chosen so that the salt bridge in the inactive state between R3.50(214) and D6.30(338) would be broken due to the movement of the intracellular end of TMH6 away from that of TMH3 and out into lipid.[52] TMH6 was also rotated (counterclockwise from extracellular view) so that Cys 6.47 became accessible from inside the binding site crevice.[14]

Preparation of Helices. Each helix of the model was capped as the acetamide at its N-terminus and as the *N*-methyl amide at its C-terminus. Ionizable residues in the first turn of either end of the helix were neutralized, as were any lipid facing charged residues. Ionizable residues were considered charged if they appeared anywhere else in the helix.

Ligand Conformations and Docking Positions. The binding-site conformations and anchoring interactions inside the receptor used for each ligand were based on our published computational and experimental work and that of others as detailed below.

SR141716A. We have recently shown in a mutant cycle study that the C3 substituent of SR141716A has a direct interaction with K3.28,[6] so K3.28 was used as the anchor point for docking. Since chimera studies have identified that the TMH4-TMH5 region of CB_1 is involved in SR141716A binding,[3] the ligand was docked in the TMH3−4−5 region of CB_1. Our SR141716A conformational analysis studies identified two principal conformers (of the C3 substituent),[6] one of which was identified as the bioactive conformer based on our mutant cycle experimental results.[6] This conformer produces the highest negative electrostatic potential in the C-3 substituent region (0.92 kcal/mol above global minimum as indicated by ab initio Hartree−Fock 6-31G* calculations). In this conformation, the piperidine ring is in a chair conformation with the nitrogen lone pair of electrons pointing in the same direction as the carboxamide oxygen. The carboxamide of the C3 substituent of SR141716A is in a trans geometry. A recent crystal structure of SR141716A confirms this carboxamide trans geometry (C. George, Laboratory for the Structure of Matter, Naval Research Laboratory, personal communication). This bioactive conformer of SR141716A was docked such that its carboxamide oxygen formed a hydrogen bond with K3.28 and the ligand occupied the TMH3−4−5 region of CB_1 without van der Waals overlaps. The resultant ligand/CB_1 complex was energy minimized as described below.

WIN55,212−2. CB_1/CB_2 chimera studies have suggested that WIN55,212−2 binds in the TMH4-TMH5 region of CB_1.[3] In agreement with these results, we have shown that the CB_1 affinity of WIN55,212−2 increases in a V5.46F mutant, suggesting that TMH5 is part of the WIN55,212−2 binding pocket.[5] WIN55212−2 was therefore docked in the TMH4−5 region of CB_1. Our synthesis of rigid indene analogues that mimic the s-cis and s-trans conformers of WIN55,212−2 suggested that the s-trans conformation of WIN55,212−2 is its bioactive conformation.[45] WIN55,212−2, in its s-trans conformation, was docked in the TM4−5 region of CB_1 using interactive computer graphics with the naphthoyl group oriented either extracellularly or intracellularly and each ligand/CB_1 complex was energy minimized. These calculations suggested that a naphthoyl intracellular orientation resulted in the lower energy complex.

Anandamide. CB_1 human K3.28(192)A mutation binding results for the endogenous agonist anandamide have suggested that K3.28 is a primary interaction site.[29] SAR studies reported by Pinto and co-workers have suggested that the carboxamide group, rather than the hydroxyl group of anandamide, is important for high CB_1 affinity.[30] We therefore used an interaction between the caboxamide oxygen and K3.28 as an anchor point for docking anandamide at CB_1. We have used the CM method, a Monte Carlo/simulated annealing method, to identify low free energy conformations of anandamide.[25,27] In contrast to SR141716A and WIN55,212−2, which have relatively few low-energy conformers, anandamide was found to have many low-energy conformations. The CM method identified two major conformational families for anandamide, a U-shaped cluster (49/100 structures) and an extended-shape cluster (29/100 structures).[25] These results combined with CM results for several acyl chain congeners of anandamide suggested that anandamide analogues (from the U-shaped cluster) that can form tightly curved structures should have the highest affinity for CB_1.[25] These results led us to select structures from the anandamide U-shaped cluster[25] for docking. A representative structure from the U-shaped cluster was selected such that when docked in our CB_1 R* model, the carboxamide oxygen of this conformer could form a hydrogen bond with K3.28 but create no van der Waals overlaps with other residues in the binding site crevice. The ligand/CB_1 complex was then energy minimized as described below.

Energy Minimization: Ligand−Receptor Complexes and Unoccupied Receptor States. Each ligand was docked using interactive computer graphics. SR141716A was docked in the inactive state (R) model of CB_1, because inverse agonists have higher affinity for this state,[6] while WIN55,212−2 and anandamide were docked in the model of the CB_1 active R* state, because agonists have higher affinity for this state. The energy of the ligand/CB_1 R or ligand/CB_1 R* TMH bundle complex was minimized using the AMBER* united atom force field in Macromodel 6.5 (Schrödinger Inc., Portland, OR). A distance dependent dielectric, 8.0 Å extended nonbonded cutoff (updated every 10 steps), 20.0 Å electrostatic cutoff, 4.0 Å hydrogen bond cutoff, and explicit hydrogens on sp^2 carbons were used. The first stage of the calculation consisted of 2000 steps of Polak-Ribier conjugate gradient (CG) minimization in which a force constant of 225 kJ/mol was used on the helix backbone atoms in order to hold the TMH backbones fixed, while the side chains were permitted to relax. The second stage of the calculation consisted of 100 steps of CG in which the force constant on the helix backbone atoms was reduced to 50 kJ/mol in order to allow the helix backbones to adjust. Stages one and two were repeated with the number of CG steps in stage two incremented from 100 to 500 steps until a gradient of 0.001 kJ/(mol·Å ^{2}) was reached. This same minimization protocol was followed for the unoccupied receptor R and R* models.

Assessment of Aromatic Stacking Interactions. Residues and/or ligand regions were designated here as participating in an aromatic stacking interaction if subject rings had centroid to centroid distances (*d*) between 4.5 and 7.0 Å. These interactions were further classified as "tilted-T" arrangements if $30° \leq \alpha \leq 90°$ and as parallel arrangements for $\alpha < 30°$ (where α is the angle between normal vectors of interacting rings). Parallel arrangements were considered favorable only if the interacting rings were offset from each other.[38] All measurements were made using Macromodel 6.5 (Schrödinger Inc.).

Mutation Studies. Materials. [^{3}H]CP55,940, SR141716A, and CP55,940 were obtained from the National Institutes on Drug Abuse. WIN55,212−2 was purchased from RBI (Natick, MA) and anandamide was purchased from Tocris. The mouse CB_1 cDNA was cloned in our lab.[53]

Mutagenesis. Mutations were introduced with the QuikChange site-directed mutagenesis kit (Stratagene) as previously described.[56] This method allows mutagenesis to be performed in any vector, hence we used mouse CB_1 subcloned into pcDNA3 (Invitrogen). The DNAs were sequenced to confirm mutation in the desired regions only. The mutations were made with the following primer sets: (forward) F3.25A(190) CAA AGA TAG TCC CAA TGT GGC TCT GTT CAA ACT GGG TGG, F3.36A(201) GTG GGG TTA CCG CCT CCG CCA CAG CAT CTG TG, W4.64A(256) CTC TCC TGG GCG CGA ACT GCA AGA AGC TGC, W5.43A(280) GAA ACC TAC CTG ATG TTC GCG ATC GGA GTC ACC AGT G, W6.48A(357) TGT TGA TCA TCT GCG CGG GCC CTC TGC TTG CGA TC. The reverse primers were the reverse complement of the forward primer sequences.

Cell Culture and Transfection. Cell lines were created by transfection of wild type or mutant CB_1pcDNA3 into HEK 293 cells by the Lipofectamine reagent (Invitrogen) and cultured as previously described.[56] Cell lines containing moderate to high levels of receptor mRNA, assessed by Northern analysis, were tested for receptor binding and signal transduction properties. Cell lines with the most similar receptor expression profile, as ascertained by B_{max} values, were chosen for further analysis (Table 2).

Cannabinoid Receptor Radioligand Binding Determinations. The current assay has been previously described.[56,57] Briefly, cells were harvested in phosphate-buffered saline containing 1 mM EDTA and centrifuged at 500*g* for 5 min. The cell pellet was homogenized and centrifuged three times at 1600*g* (10 min). The combined supernatants were centrifuged at 100 000*g* (60 min). The pellet (P2 membrane) was resuspended in 3 mL of buffer B (50 mM Tris-HCl, 1 mM EDTA, 3 mM $MgCl_2$, pH 7.4) to yield a protein concentration of approximately 1 mg/mL. Binding was initiated by the addition of 25−75 μg of P2 membrane protein to silanized tubes containing [^{3}H]CP55,940 (102.9 Ci/mmol) and a sufficient volume of buffer C [50 mM Tris-HCl, 1 mM EDTA, 3 mM $MgCl_2$, and 5 mg/mL fatty acid free bovine serum albumin (BSA), pH 7.4] to bring the total volume to 0.5 mL. The addition of 1 μM of unlabeled CP55,940 was used to assess nonspecific binding. Specific binding averaged >50% of total binding in all cell lines used in the analysis. Following incubation (30 °C for 1 h), binding was terminated by the addition of 2 mL of ice cold buffer D (50 mM Tris-HCl, pH 7.4, plus 1 mg/mL BSA) and rapid vacuum filtration through Whatman GF/C filters (pretreated with 0.1% polyethyleneimine for at least 2 h). CP55,940 and all cannabinoid analogues were prepared by suspension in assay buffer from a 1 mg/mL ethanolic stock without evaporation of the ethanol (final concentration of no more than 0.4%). When anandamide was used as a displacing ligand, experiments were performed in the presence of phenylmethylsulfonyl fluoride to inhibit the break down of the ligand by endogenous esterases (50 μM). Saturation experiments were conducted with six concentrations of [^{3}H]CP55,940 ranging from 250 pM to 10 nM. Competition assays were conducted with 1 nM [^{3}H]CP55,940 and six concentrations (0.001 nM to 10 μM) displacing ligands. B_{max} and K_d values were calculated by unweighted least-squares nonlinear regression of log concentration values versus binding of pmol/mg protein. These data was fit to a one-site binding model using GraphPad Prism (GraphPad). Displacement IC_{50} values were determined by unweighted least-squares nonlinear regression of log concentration-percent displacement data and then converted to K_i values using the method of Cheng and Prusoff[58] and analyzed with GraphPad Prism.

Immunocytochemistry. Cells were plated onto cover slips that had been pretreated for 1 h with poly D-lysine (0.02 mg/mL; Sigma) and maintained in a humidified atmosphere of 5% CO_2 in air at 37 °C. Cells were washed with 10 mM HEPES-buffered saline (comprising in mM: NaCl 130, D-glucose 25, HEPES 10, KCl 5.4, $CaCl_2$ 1.8, $MgCl_2$ 1) at room temperature and incubated for 1 h with a polyclonal rabbit anti-CB_1 receptor antibody (Cayman Chemical) at a final concentration of 8 μg/mL. Cells were washed three times with HEPES-buffered saline and fixed with 4% paraformaldehyde for 10 min at room temperature. CB_1 receptor antibody was labeled for 40 min at room temperature with Alexa Fluor 488 goat anti-rabbit secondary antibody (1:500; Molecular Probes) followed by three washes in buffer. Cover slips were mounted on slides in Vectashield (Vector Laboratories) and cell surface labeling was visualized with a fluorescence microscope (Nikon). Wild-type CB_1 expressing cells or transient cells that were transfected with W4.64A mutant CB_1 receptors were labeled. Time after transfection did not alter the labeling as a similar pattern of labeling was observed when stable or transient cells transfected with wild-type mouse CB_1 receptor were labeled. In control experiments, no labeling was observed with the secondary antibody alone or when the primary antibody was incubated with CB_1 receptor blocking peptide at 100 μg/mL (Cayman Chemical).

Statistical Analyses. The K_i and K_d values in the mutant versus wild-type cell lines were compared by analysis of logged data (GraphPad Prism) using analysis of variance (ANOVA) or the unpaired Student's *t*-test, where suitable. Bonferroni−Dunn post-hoc analyses were conducted when appropriate. *P* values <0.05 defined statistical significance.

Acknowledgment. The authors wish to thank Beverly Brookshire for her technical assistance in the preparation of the manuscript. This work was supported by National Institute on Drug Abuse grants DA05274 and DA09978 (to M.E.A.) and DA03934 and DA00489 (to P.H.R.).

References

(1) Onaivi, E. *The Biology of Marijuana: From Gene to Behaviour*; Harwood Academic Publishers: Reading, U.K., 2002.

(2) Shire, D.; Calandra, B.; Delpech, M.; Dumont, X.; Kaghad, M.; Fur, G. L.; Caput, D.; Ferrara, P. Structural features of the central cannabinoid CB_1 receptor involved in the binding of the specific CB_1 antagonist SR 141716A. *J. Biol. Chem.* **1996**, *271*, 6941−6946.

(3) Shire, D.; Calandra, B.; Bouaboula, M.; Barth, F.; Rinaldi-Carmona, M.; Casellas, P.; Ferrara, P. Cannabinoid receptor interactions with the antagonists SR 141716A and SR 144528. *Life Sci.* **1999**, *65*, 627−635.

(4) Chin, C. N.; Murphy, J. W.; Huffman, J. W.; Kendall, D. A. The third transmembrane helix of the cannabinoid receptor plays a role in the selectivity of aminoalkylindoles for CB_2, peripheral cannabinoid receptor. *J. Pharmacol. Exp. Ther.* **1999**, *291*, 837−844.

(5) Song, Z. H.; Slowey, C. A.; Hurst, D. P.; Reggio, P. H. The difference between the CB(1) and CB(2) cannabinoid receptors at position 5.46 is crucial for the selectivity of WIN55212−2 for CB(2). *Mol. Pharmacol.* **1999**, *56*, 834−840.

(6) Hurst, D. P.; Lynch, D. L.; Barnett-Norris, J.; Hyatt, S. M.; Seltzman, H. H.; Zhong, M.; Song, Z. H.; Nie, J.; Lewis, D.; Reggio, P. H. *N*-(Piperidin-1-yl)-5-(4-chlorophenyl)-1-(2,4-dichlorophenyl)-4-methyl-1 H−pyrazole-3-carboxamide (SR141716A) Interaction with LYS 3.28(192) Is Crucial for Its Inverse Agonism at the Cannabinoid CB_1 Receptor. *Mol. Pharmacol.* **2002**, *62*, 1274−1287.

(7) McAllister, S. D.; Tao, Q.; Barnett-Norris, J.; Buehner, K.; Hurst, D. P.; Guarnieri, F.; Reggio, P. H.; Nowell Harmon, K. W.; Cabral, G. A.; Abood, M. E. A critical role for a tyrosine residue in the cannabinoid receptors for ligand recognition. *Biochem. Pharmacol.* **2002**, *63*, 2121−2136.

(8) Shi, L.; Liapakis, G.; Xu, R.; Guarnieri, F.; Ballesteros, J. A.; Javitch, J. A. Beta2 adrenergic receptor activation. Modulation of the proline kink in transmembrane 6 by a rotamer toggle switch. *J. Biol. Chem.* **2002**, *277*, 40989−40996.

(9) Barnett-Norris, J.; Hurst, D. P.; Buehner, K.; Ballesteros, J. A.; Guarnieri, F.; Reggio, P. H. Agonist Alkyl Tail Interaction with Cannabinoid CB_1 Receptor V6.43/I6.46 Groove Induces a Helix 6 Active Conformation. *Int. J. Quantum Chem.* **2002**.

(10) Farrens, D.; Altenbach, C.; Ynag, K.; Hubbell, W.; Khorana, H. Requirement of rigid-body motion of transmembrane helices for light activation of rhodopsin. *Science* **1996**, *274*, 768−770.

(11) Gether, U.; Lin, S.; Ghanouni, P.; Ballesteros, J.; Weinstein, H.; Kobilka, B. Agonists induce conformational changes in transmembrane domains III and VI of the beta2 adrenoceptor. *EMBO J.* **1997**, *16*, 6737−6747.

(12) Ghanouni, P.; Steenhuis, J. J.; Farrens, D. L.; Kobilka, B. K. Agonist-induced conformational changes in the G-protein-coupling domain of the beta 2 adrenergic receptor. *Proc. Natl. Acad. Sci. U.S.A.* **2001**, *98*, 5997−6002.

(13) Jensen, A. D.; Guarnieri, F.; Rasmussen, S. G.; Asmar, F.; Ballesteros, J. A.; Gether, U. Agonist-induced conformational changes at the cytoplasmic side of transmembrane segment 6 in the beta 2 adrenergic receptor mapped by site-selective fluorescent labeling. *J Biol. Chem.* **2001**, *276*, 9279−9290.

(14) Javitch, J. A.; Fu, D.; Liapakis, G.; Chen, J. Constitutive activation of the b2 adrenergic receptor alters the orientation of its sixth membrane-spanning segment. *J. Biol. Chem.* **1997**, *272*, 18546−18549.

(15) Hulme, E. C.; Lu, Z. L.; Ward, S.; Allman, K.; Curtis, C. The conformational switch in 7-transmembrane receptors: the muscarinic receptor paradigm. *Eur. J. Pharmacol.* **1999**, *375*, 247−260.

(16) Leff, P. The two-state model of receptor activation. *Trends Pharmacol. Sci.* **1995**, *16*, 89−97.

(17) Samama, P.; Pei, G.; Costa, T.; Cotecchia, S.; Lefkowitz, R. J. Negative antagonists promote an inactive conformation of the beta 2-adrenergic receptor. *Mol. Pharmacol.* **1994**, *45*, 390−394.

(18) Burley, S.; Petsko, G. Aromatic−aromatic interaction: A mechanism of protein structure stabilization. *Science* **1985**, *229*, 23−28.

(19) Bouaboula, M.; Perrachon, S.; Milligan, L.; Canat, X.; Rinaldi-Carmona, M.; Portier, M.; Barth, F.; Calandra, B.; Pecceu, F.; Lupker, J.; Maffrand, J.-P.; LeFur, G.; Casellas, P. A selective inverse agonist for central cannabinoid receptor inhibits mitogen-activated protein kinase activation stimulated by insulin or insulin-like growth factor 1. *J. Biol. Chem.* **1997**, *272*, 22330−22339.

(20) Pan, X.; Ikeda, S.; Lewis, D. SR 141716A acts as an inverse agonist to increase neuronal voltage-dependent Ca2+ currents by reversal of tonic CB_1 cannabinoid receptor activity. *Mol Pharmacol* **1998**, *54*, 1064−1072.

(21) Meschler, J. P.; Kraichely, D. M.; Wilken, G. H.; Howlett, A. C. Inverse agonist properties of *N*-(piperidin-1-yl)-5-(4-chlorophenyl)-1-(2,4-dichlorophenyl)-4-methyl-1H-pyrazole-3-carboxamide HCl (SR141716A) and 1-(2-chlorophenyl)-4-cyano-5-(4-methoxyphenyl)-1H-pyrazole-3-carboxylic acid phenylamide (CP-272871) for the CB(1) cannabinoid receptor. *Biochem. Pharmacol.* **2000**, *60*, 1315−1323.

(22) Thomas, B. F.; Gilliam, A. F.; Burch, D. F.; Roche, M. J.; Seltzman, H. H. Comparative receptor binding analyses of cannabinoid agonists and antagonists. *J. Pharmacol. Exp. Ther.* **1998**, *285*, 285−292.

(23) Katoch-Rouse, R.; Pavlova, O. A.; Caulder, T.; Hoffman, A. F.; Mukhin, A. G.; Horti, A. G. Synthesis, structure−activity relationship, and evaluation of SR141716 analogues: Development of central cannabinoid receptor ligands with lower lipophilicity. *J. Med. Chem.* **2003**, *46*, 642−645.

(24) D'Ambra, T. E.; Estep, K. G.; Bell, M. R.; Eissenstat, M. A.; Josef, K. A.; Ward, S. J.; Haycock, D. A.; Baizman, E. R.; Casiano, F. M.; Beglin, N. C. Conformationally restrained analogues of pravadoline: nanomolar potent, enantioselective, (aminoalkyl)-indole agonists of the cannabinoid receptor. *J. Med. Chem.* **1992**, *35*, 124−135.

(25) Barnett-Norris, J.; Hurst, D. P.; Lynch, D. L.; Guarnieri, F.; Makriyannis, A.; Reggio, P. H. Conformational memories and the endocannabinoid binding site at the cannabinoid CB_1 receptor. *J. Med. Chem.* **2002**, *45*, 3649−3659.

(26) Palczewski, K.; Kumasaka, T.; Hori, T.; Behnke, C. A.; Motoshima, H.; Fox, B. A.; Le Trong, I.; Teller, D. C.; Okada, T.; Stenkamp, R. E.; Yamamoto, M.; Miyano, M. Crystal structure of rhodopsin: A G protein-coupled receptor. *Science* **2000**, *289*, 739−745.

(27) Barnett-Norris, J.; Guarnieri, F.; Hurst, D. P.; Reggio, P. H. Exploration of biologically relevant conformations of anandamide, 2-arachidonylglycerol, and their analogues using conformational memories. *J. Med. Chem.* **1998**, *41*, 4861−4872.

(28) LaLonde, J. M.; Levenson, M. A.; Roe, J. J.; Bernlohr, D. A.; Banaszak, L. J. Adipocyte lipid-binding protein complexed with arachidonic acid. Titration calorimetry and X-ray crystallographic studies. *J. Biol. Chem.* **1994**, *269*, 25339−25347.

(29) Song, Z.-H.; Bonner, T. I. A lysine residue of the cannabinoid receptor is critical for receptor recognition by several agonists but not WIN55212−2. *Mol. Pharmacol.* **1996**, *49*, 891−896.

(30) Pinto, J. C.; Potie, F.; Rice, K. C.; Boring, D.; Johnson, M. R.; Evans, D. M.; Wilken, G. H.; Cantrell, C. H.; Howlett, A. C. Cannabinoid receptor binding and agonist activity of amides and esters of arachidonic acid. *Mol. Pharmacol.* **1994**, *46*, 516−522.

(31) Hillard, C. J.; Manna, S.; Greenberg, M. J.; DiCamelli, R.; Ross, R. A.; Stevenson, L. A.; Murphy, V.; Pertwee, R. G.; Campbell, W. B. Synthesis and characterization of potent and selective agonists of the neuronal cannabinoid receptor (CB_1). *J. Pharmacol. Exp. Ther.* **1999**, *289*, 1427−1433.

(32) Bonechi, C.; Brizzi, A.; Brizzi, V.; Francoli, M.; Donati, A.; Rossi, C. Conformational Analysis of *N*-arachidonylethanolamide (Anandamide) Using Nuclear Magnetic Resonance and Theoretical Calculations. *Magn. Reson. Chem.* **2001**, *39*, 432−437.

(33) Barnett-Norris, J.; Hurst, D. P.; Reggio, P. H. The influence of cannabinoid receptor second extracellular loop conformation on the binding of CP55940. *2003 Symposium on the Cannabinoids*; International Cannabinoid Research Society, Burlington, VT: Cornwall, Ontario, Canada, 2003; p 78.

(34) Rhee, M.-H.; Nevo, I.; Bayewitch, M. L.; Zagoory, O.; Vogel, Z. Functional role of tryptophan residues in the fourth transmembrane domain of the CB_2 cannabinoid receptor. *J. Neurochem.* **2000**, *75*, 2485−2491.

(35) Ward, W. H.; Timms, D.; Fersht, A. R. Protein engineering and the study of structure−function relationships in receptors. *Trends. Pharmacol. Sci.* **1990**, *11*, 280−284.

(36) Sansom, M. S.; Weinstein, H. Hinges, swivels and switches: the role of prolines in signaling via transmembrane alpha-helices. *Trends. Pharmacol. Sci.* **2000**, *21*, 445−451.

(37) Ballesteros, J. A.; Deupi, X.; Olivella, M.; Haaksma, E. E.; Pardo, L. Serine and threonine residues bend alpha-helices in the chi-(1) = g(−) conformation. *Biophys. J.* **2000**, *79*, 2754−2760.

(38) Hunter, C.; Singh, J.; Thornton, J. π−π interactions: The geometry and energetics of phenylalanine-phenylalanine interactions in proteins. *J. Mol. Biol.* **1991**, 218.

(39) Sinnokrot, M. O.; Valeev, E. F.; Sherrill, C. D. Estimates of the ab initio limit for pi-pi interactions: The benzene dimer. *J. Am. Chem. Soc.* **2002**, *124*, 10887−10893.

(40) Lan, R.; Liu, Q.; Fan, P.; Lin, S.; Fernando, S. R.; McCallion, D.; Pertwee, R.; Makriyannis, A. Structure−activity relationships of pyrazole derivatives as cannabinoid receptor antagonists. *J. Med. Chem.* **1999**, *42*, 769−776.

(41) Wiley, J. L.; Jefferson, R. G.; Grier, M. C.; Mahadevan, A.; Razdan, R. K.; Martin, B. R. Novel pyrazole cannabinoids: insights into CB(1) receptor recognition and activation. *J. Pharmacol. Exp. Ther.* **2001**, *296*, 1013−1022.

(42) Shim, J. Y.; Welsh, W. J.; Cartier, E.; Edwards, J. L.; Howlett, A. C. Molecular interaction of the antagonist *N*-(piperidin-1-yl)-5-(4-chlorophenyl)-1-(2,4-dichlorophenyl)-4-methyl-1H-pyrazole-3-carboxamide with the CB_1 cannabinoid receptor. *J. Med. Chem.* **2002**, *45*, 1447−1459.

(43) Huffman, J.; Dai, D.; Martin, B.; Compton, D. Design, Synthesis and Pharmacology of Cannabimimetic Indoles. *Bioorg. Med. Chem. Lett.* **1994**, *4*, 563−566.

(44) Eissenstat, M. A.; Bell, M. R.; D'Ambra, T. E.; Alexander, E. J.; Daum, S. J.; Ackerman, J. H.; Gruett, M. D.; Kumar, V.; Estep, K. G.; Olefirowicz, E. M. Aminoalkylindoles: structure−activity relationships of novel cannabinoid mimetics. *J. Med. Chem.* **1995**, *38*, 3094−3105.

(45) Reggio, P. H.; Basu-Dutt, S.; Barnett-Norris, J.; Castro, M. T.; Hurst, D. P.; Seltzman, H. H.; Roche, M. J.; Gilliam, A. F.; Thomas, B. F.; Stevenson, L. A.; Pertwee, R. G.; Abood, M. E. The bioactive conformation of aminoalkylindoles at the cannabinoid CB_1 and CB_2 receptors: Insights gained from (E)- and (Z)-naphthylidene indenes. *J. Med. Chem.* **1998**, *41*, 5177−5187.

(46) Huffman, J.; Mabon, R.; Wua, M.-J.; Lu, J.; Hart, R.; Hurst, D.; Reggio, P.; Wiley, J.; Martin, B. 3-Indolyl-1-naphthylmethanes: New Cannabimimetic Indoles Provide Evidence for Aromatic Stacking Interactions with the CB_1 Cannabinoid Receptor. *Bioorg. Med. Chem.* **2003**, *11*, 539−549.

(47) Brandl, M.; Weiss, M. S.; Jabs, A.; Suhnel, J.; Hilgenfeld, R. C−H···[pi]-Interactions in Proteins. *J. Mol. Biol.* **2001**, *307*, 357−377.

(48) Bracey, M. H.; Hanson, M. A.; Masuda, K. R.; Stevens, R. C.; Cravatt, B. F. Structural adaptations in a membrane enzyme that terminates endocannabinoid signaling. *Science* **2002**, *298*, 1793−1796.

(49) Malkowski, M. G.; Ginell, S. L.; Smith, W. L.; Garavito, R. M. The productive conformation of arachidonic acid bound to prostaglandin synthase. *Science* **2000**, *289*, 1933−1937.
(50) Ballesteros, J. A.; Weinstein, H. Integrated methods for the construction of three-dimensional models and computational probing of structure function relations in G protein-coupled receptors. *Methods in Neuroscience*; Academic Press: San Diego, 1995; pp 366−428.
(51) Lin, S.; Sakmar, T. Specific tryptophan UV-absorbance changes are probes of the transition of rhodopsin to its active state. *Biochemistry* **1996**, *35*, 11149−11159.
(52) Ballesteros, J.; Jensen, A.; Liapakis, G.; Rasmussen, S.; Shi, L.; Gether, U.; Javitch, J. Activation of the β_2 adrenegic receptor involves disruption of an ionic link between the cytoplasmic ends of transmembrane segments 3 and 6. *J. Biol. Chem.* **2001**, *276*, 29171−29177.
(53) Abood, M. E.; Ditto, K. E.; Noel, M. A.; Showalter, V. M.; Tao, Q. Isolation and expression of a mouse CB_1 cannabinoid receptor gene. *Biochem. Pharmacol.* **1997**, *53*, 207−214.
(54) Bramblett, R. D.; Panu, A. M.; Ballesteros, J. A.; Reggio, P. H. Construction of a 3D model of the cannabinoid CB_1 receptor: Determination of helix ends and helix orientation. *Life Sci.* **1995**, *56*, 1971−1982.
(55) Gerard, C. M.; Mollereau, C.; Vassart, G.; Parmentier, M. Molecular cloning of a human cannabinoid receptor which is also expressed in testis. *Biochem. J.* **1991**, *279*, 129−134.
(56) Tao, Q.; McAllister, S. D.; Andreassi, J.; Nowell, K. W.; Cabral, G. A.; Hurst, D. P.; Bachtel, K.; Ekman, M. C.; Reggio, P. H.; Abood, M. E. Role of a conserved lysine residue in the peripheral cannabinoid receptor (CB_2): Evidence for subtype specificity. *Mol. Pharmacol.* **1999**, *55*, 605−613.
(57) Tao, Q.; Abood, M. E. Mutation of the highly conserved aspartate residue in the CB_1 and CB_2 receptors disrupts G-protein coupling. *J. Pharmacol. Exp. Ther.* **1998**, *285*, 651−658.
(58) Cheng, Y. C.; Prusoff, W. H. Relationships between the inhibition constant (Ki) and the concentration of inhibitor that causes 50% inhibition (IC50) on an enzymatic reaction. *Biochem Pharmacol* **1973**, *22*, 3099−3108.

JM0302647